

Fault kinematics and stress fields in the Rwenzori Mountains, Uganda

Abstract

The Rwenzori Mountains in western Uganda form an active rift transfer zone in the Western Branch of the East African Rift System. Here we quantify local stress fields in high resolution from field observations of fault structures to shed light on the complex, polyphase tectonics expected in transfer zones. We apply the Multiple Inverse Method, which is optimized for heterogeneous fault-slip data, to the northern and central Rwenzori Mountains. Observations from the northern Rwenzori Mountains show larger heterogeneity than data from the central Rwenzori, including unexpected compressional features, thus the local stress field indicates polyphase transpressional tectonics. We suggest transpression here is linked to rotational and translational movements of the neighboring Victoria block relative to the Rwenzori block that includes strong overprinting relationships. Stress inversions of data from the central Rwenzori Mountains indicate two distinct local stress fields. These results suggest the Rwenzori block consists of smaller blocks.

Introduction

The Rwenzori Mountains are the highest non-volcanic mountains in Africa, located in a rift-transfer zone within the northern Western Branch of the East African Rift System (EARS).

Rift-transfer zones caused by along-strike segmentation are common features of continental rift systems (e.g. Bosworth, 1984; Morley and Nelson, 1990; Foster and Nimmo 1996), usually leading to en-echelon stepping of laterally continuous rift segments. Stress-fields related to these structures are complex and can yield valuable insight into the major and minor forces acting in the region (Delvaux and Barth, 2009). Geological structures that develop in active rift-transfer zones include rift basin inversions, reverse faulting in a region with a dominant tensile regime, and polyphase fault/slip (Macdonald, Scheirer, and Carbotte 1991; Moustafa 1997; Shan, Li, and Lin 2004). These structures cannot be explained by a singular uniform

24 stress-field.

25 Advancing our knowledge of local stress fields associated with rift-transfer zones will provide constraints on
26 local kinematics that are needed to understand the dynamics and the relevant factors for their tectonic
27 evolution. Here, we present new, high-resolution fault-slip data from the Rwenzori area and perform stress
28 inversion calculations with these data sets. Local data sets were collected in small, clearly defined areas, and
29 are interpreted with regard to the plate tectonic setting of the Rwenzori microplate.

30 **Geology and kinematics of the Rwenzori Mountains**

31 **Geology and Structure**

32 The Rwenzori Mountains form a 100 km long, 50 km wide horst block, bounded by en-echelon faults. The
33 mountain range is situated within a rift-transfer zone, which connects two rift segments of the Albertine Rift.
34 The Albertine Rift forms the northern part of the western Branch of the EARS.

35 The northern Rwenzori area and the Rwenzori block itself are comprised of gneisses from the Archaean
36 Gneissic Granulite Complex that are interlayered with metasediments (schist, amphibolites and quartzites)
37 associated with the paleo-Proterozoic Buganda-Toro Belt (Figure 1). In the southern Rwenzori region, also
38 argillaceous sediments of the meso-proterozoic Kibaran Belt appear.

39 The Rwenzori block is bounded by a number of major border faults and fault networks, which separates it
40 from the surrounding plates and rift grabens. In the west, the block is bounded by the Bwamba normal fault,
41 which dips towards the Semliki rift valley (Koehn et al. 2008)□. Along this line, the Rwenzori block is
42 completely detached from the adjacent Congo craton.

43 The situation in the NE, where the Rwenzori block is bounded by the NNE striking Ruimi-Wasa fault, is
44 slightly more complicated. In the very N the Ruimi-Wasa fault borders against a fully developed rift basin,
45 and branches out with a NE striking major fault N of Fort Portal (see Figure 2 and Figure 3). In its central to
46 northern central range (between c. N0°40' and N0°20') the Rwenzori block is still in contact with the the
47 Tanzania craton in its east (Figure 2 and 3). Towards the central Rwenzoris, the Ruimi-Wasa fault is replaced
48 by the NNW-SSE striking Kisomoro fault. Seismic fault plane solutions (Figure 2) indicate that the dominant

49 displacement on the Kisomoro fault is normal. The S of the Rwenzori horst is segmented by several NE-SW
50 striking large scale normal faults.

51 Detailed structural mapping of mainly smaller brittle faults in the Rwenzori mountains reveals complex fault
52 systems in the central Rwenzoris (Koehn et al. 2008; Link et al. 2010)□. Polyphase stress fields induced
53 northwards directed thrusting, at least two strike slip events with roughly N–S and E–W compression and
54 SW-NE striking normal faults (Sachau, Koehn, and Passchier 2011)□. Figure 2 includes a schematic
55 overview over these fault systems. The data can be resolved into two small to medium scale fault
56 populations: range-parallel faults that are oriented parallel to the main normal faults around the Rwenzori
57 range and trans section faults crosscutting the central Rwenzoris at various angles. It has been proposed that
58 the center of the Rwenzoris has been also segmented by large scale faults, similar to the situation in the S
59 (Ring, 2008)□.

60 Figure 2 displays major brittle structures, along with a number of selected fault plane solutions of seismic
61 events in the area, which have been acquired by Lindenfeld et al. (2012). The displayed solutions indicate the
62 large heterogeneity of the present day stress field in the Rwenzori area. The stress field is further discussed in
63 later sections.

64 Pre-rift paleo-stresses and brittle structures in the Rwenzori area are not well known. The EARS in general
65 has a poly-phase brittle deformation history, and it can be assumed that this is true for the Rwenzori area as
66 well. Older pre-rift brittle faults may be present in the Rwenzori mountains. Delvaux et al. (2012) mention
67 two brittle events in the Rukwa basin south of the Albertine rift, one event being compressional and the
68 second event strike slip. Especially the steep reverse faults in the centre of the Rwenzori mountains that
69 indicate NNW directed shorting may represent one of these pre-rift events.

70 Figure 4 shows typical faults from the area, which are typically either in metamorphic host rocks or in
71 young, little consolidated sediments (here volcanic ash).

72 Cross-cutting relationships of faults in the Rwenzori mountains are not always clear, so that it is not straight
73 forward to produce detailed age relationships of faults. The best cross-cutting relationships are visible in the
74 northern part of the Rwenzori mountains where rift related normal faulting is older than strike slip and
75 oblique slip faulting. This relation can be seen in several locations in the north where shallow to horizontal
76 striations and slicken-fibres overprint steep ones. The youngest faults in the NE corner of the northern part of
77 the Rwenzori mountains are steep reverse faults that either overprint strike slip faulting or is coeval to strike

78 slip faulting. Age relationships of faults in the centre of the Rwenzori mountains are not clear, however
79 faulting in the Kilembe mine indicates that oblique slip movements have been active within the last 30 years
80 with one fault showing an estimated slip rate of 0.5 mm/year.

81 **Active Kinematics**

82 The Albertine Rift System forms the northern part of the Western branch of the East African Rift System
83 (EARS) located between the Nubian plate to the west and the Victoria block to the east (Figure 3a). The
84 Victoria block encompasses the Tanzania craton and is bounded by Proterozoic mobile belts (i.e. Fernandes
85 et al., 2013). The Nubian plate can be identified with the region west of the EARS following previously
86 defined boundaries of the African plate (Horner-Johnson et al., 2005), including the Congo craton. Since the
87 Rwenzori block itself is enclosed by major faults, we consider it a microplate. Here, we use the terms block
88 and microplate as synonyms.

89 Geodetic studies indicate that the Victoria plate between the Western and Eastern Rifts of the EARS rotates
90 anti-clockwise with respect to the Nubian plate with the Albertine rift opening with a velocity of
91 approximately 2.1 mm per year in an ESE direction (e.g. Stamps et al., 2008; Fernandes et al., 2013; Saria et
92 al., 2014). Structural and seismic data used to test numerical models indicate the Rwenzori block itself
93 rotates clockwise (Koehn et al. 2010; Figure 3a). These authors suggest the Rwenzori block is detached
94 from the neighboring plates in the south, but still attached to the Victoria block in the north. The Rwenzori
95 block may be tilted along a NNE-SSW trending axis, with the highest peak to the west (Osmaston 1989;
96 Taylor and Howard 1998), however the southern third of the Rwenzori block does not seem to be affected
97 by this tilt (Koehn et al. (2010), Bauer et al. (2013)).

98 The Western Rift of the EARS system is split into several 100-300 km length segments (e.g. Morley and
99 Nelson 1990; Ebinger 1989). These segments are initiated with the onset of sediment deposition from which
100 rift propagation ensues.

101 The Rwenzori Mountains act as a rift transfer zone at the intersection of two rift segments, the southern
102 segment of the Albertine rift system near Lake Edwards to the south of the Rwenzori Mountains and a
103 segment to the north near Lake Albert. Koehn et al. (2008, 2010) suggest these segments migrated towards

104 each other and captured the Rwenzori basement block (Figure 2b). Block capturing of this type also occurs
105 in other locations within the EARS such as the Mbeya Mountains in Tanzania and the Amaro Horst in
106 Ethiopia (Bahat and Paul 1987)□.

107 The southern Western Branch began opening 25 Mya (Roberts et al., 2012), but the timing of the northern
108 Western Branch opening and capture of the Rwenzori block is still under debate. Previous research by Koehn
109 et al. (2010), which is based on numerical models, suggests 3 main stages. Following Figure 3b: Stage I
110 began approximately 15 Ma and continued for about 2 Ma. During this stage the rift segments to the north
111 and south of the present-day Rwenzori Mountains were initiated. In Stage II, which lasted approximately 4
112 Ma, the two rift segments propagated towards each other. The Rwenzori block rotates clockwise, because it
113 is still attached to the Nubia plate in the west and the Victoria plate in the north. In Stage III, which began 8-
114 10 Ma ago, the present-day Rwenzori block forms and becomes detached from the adjacent plates except in
115 the northeast, where it is still attached to the Victoria block and detachment is still ongoing.

116 **Materials and Methods**

117 ***Stress inversion methods***

118 Two different methods have been proposed in order to calculate stress fields from fault slip data: the
119 PBT method (Turner 1953)□ and the Direct Inversion method (Angelier 1990)□.

120 The PBT method is based on the Mohr-Coulomb fracture criterion and calculates stresses from the
121 orientation of single fault planes, where P is the axis of contraction, T the extension axis and B is the neutral
122 axis in the fault plane. Most studies identify the P-axis with σ_1 , B with σ_2 and T with σ_3 (Sippel et al. 2009)□.

123 The angle of internal friction (θ) is assumed to equal 30° in this study, as recommended for most geological
124 materials in the crust (Sippel et al. 2009)□. The PBT methods considers all faults as being formed and moved
125 by the same stress field and ignores possible fault reactivation, which is an important shortcoming if applied
126 to heterogeneous stress fields.

127 The Direct Inversion Method is based on the Wallace-Bott hypothesis, which assumes that slip occurs in the
128 direction parallel to the resolved shear stress on the fault plane (τ), which in turn is determined by the

129 orientation of the traction vector . Once a stress tensor σ is assumed, a slip direction on a given fault plane
130 can be calculated and a misfit angle with the observed slip direction can be determined. The state of stress of
131 a homogeneous stress field is then calculated by a minimization routine of the misfit angle for a sufficient
132 number of fault-slip data.

133 This study employs mainly the Multiple Inverse Method (MIM), which is optimized for highly
134 heterogeneous fault-slip data as found in the Rwenzori area. The Multiple Inversion extends the scheme of
135 the Direct Inversion Method. MIM extracts subsets with k elements from a given set of fault-slip data and
136 applies a classical direct stress inversion as described above to the given subsets. The so-called fault-
137 combination number k is given by the user and is usually in the range between $k=3$ and $k=8$. The number of
138 subsets is given by the binomial coefficient of k and the total number of fault-slip data. As a result, correct
139 stress states are expected to get a large number of 'votes' from the stress inversion on the subsets.

140 When applying the Multiple Inverse Method to a data set, we calculated the results for $k=3$, $k=4$ and $k=5$ in
141 order to test the stability of the clusters. The displayed MIM plots were calculated with $k=5$, as
142 recommended by the authors of the method (Yamaji 2000)□.

143 We used the software TectonicsFP (Reiter and Acs 2003)□ to perform PBT and DIM calculations. The
144 Multiple Inverse Method was applied using the *Multiple Inverse Method Software Package* (Otsubo and
145 Yamaji 2006; Yamaji 2000)□.

146 It is preferable to restrict stress inversion methods to data sets of small sized areas, preferably on the outcrop
147 scale, but certainly not on the regional scale (Pollard, Saltzer, and Rubin 1993; Homberg et al. 1996; Tikoff
148 and Wojtal 1999)□.

149 ***Data acquisition and sample localities***

150 The fault plane data and fault-slip data used in this study have been acquired during field campaigns over the
151 past years. Existing data sets of the central Rwenzoris and of the northern Rwenzoris could be significantly
152 improved and expanded during the last campaign in 2012. Thanks to road construction works for the new tar
153 road from Fort Portal to Bundibugyo it was it was for the first time possible to acquire a significant number

154 of fault-slip data from the NE.

155 For this study we evaluated fault-slip data from a domain in the NE Rwenzoris, and from a domain in the
156 central Rwenzoris (see Figure 5 for sample localities). 223 fault plane orientations from the central part of
157 the Rwenzoris and 120 fault planes from the very N of the Rwenzoris were used. Stress inversion at four
158 localities in the very N is based on a total of 117 fault-slip data, and on a total of 63 fault-slip data from 3
159 locations in the central Rwenzoris. Figure 6 gives an overview over the complete set of fault-slip data.

160 Individual data sets used for stress inversion consist of 18 to 43 fault-slip data, which we considered to be a
161 suitable for the applied stress inversion method (Multi Inverse Method, see below). The size of measured
162 faults is typically on outcrop scale. Figure 4a shows a typical fault surface.

163 Each stress inversion was performed for the smallest possible area. In the N, the outcrop situation was partly
164 good enough to collect sufficiently large fault-slip datasets for single outcrops. This was not possible in the
165 high Rwenzoris, where the collected data represent localities in the immediate vicinity of Bujuku Hut,
166 Kitandara Hut and Elena Hut (Figure 5).

167 Fault data from the northern domain have been acquired at eight different outcrops along an approximately
168 N-S profile over a distance of 18 km, along the NE boundary of the Rwenzori block. The profile is of
169 particular interest, because it covers a line from where the rift graben is already fully developed (location
170 BF1 in Figure 5) to a location where the Rwenzori block is still connected to the Victoria plate (location BF7
171 / BF8 in Figure 5).

172 **Results**

173 In this section we present structural data and the results of the stress inversion. In case of stress inversion, we
174 display and interpret mainly results from the MIM method, which is best fitted to deal with the large
175 heterogeneity of the fault-slip data in the Rwenzori area. The heterogeneity is both, spatial and temporal,
176 meaning that variations of the recorded stress state occur between neighboring outcrops as well as in the
177 fault-slip data of individual outcrops.

178 The large temporal variation of local stress fields, further discussed below, leads to frequent reactivation of

179 existing fault planes, combined with the creation of new fault planes. In effect, the scatter in PBT results of
180 large data sets is considerable and makes the detection of meaningful clusters highly speculative. Further
181 more, slip indicators on fault surfaces are usually not genetically related to the related fault plane, which
182 distorts results from the PBT method even further.

183 A similar argument prevents an analysis of the data by Direct Inversion, since the method yields meaningful
184 results only if a set of at least four genetically related slip indicators is analyzed. The required genetic
185 relation can usually not be guaranteed.

186 **Presentation**

187 PBT results are shown as plots of the kinematic axes for every fault datum of the data set in a lower
188 hemisphere stereo net (Figure 7). P is the axis of compression, T the axis of extension and B the neutral axis.
189 Occasionally, also the mean vectors and the associated cones of confidence with a significance of 99% are
190 given. Results of the Direct Inversion are indicated by the principal stress axes plotted on a lower hemisphere
191 stereogram (Figure 7).

192 Results of the Multiple Inverse Method are shown as poles of the principal stress axes σ_1 and σ_3 , plotted to
193 separate lower hemisphere stereograms. Colors indicate the value of $\Phi = (\sigma_2 - \sigma_3) / (\sigma_1 - \sigma_3)$ (Figure 8a
194 and Figure 9a), which describes the state of stress. $\Phi = 0$ and $\Phi = 1$ indicate an axial state of stress, with
195 $\sigma_1 > \sigma_2 = \sigma_3$ or Θ , respectively. A triaxial state of stress is indicated if $0 < \sigma_1 < 1$. Steep (inclination of $>$
196 45°) Θ or σ_3 axes indicate normal or reverse faulting, respectively, while a steep σ_2 axis is a sign for strike
197 slip faulting.

198 Statistical fault plane data are shown in lower hemisphere stereo plots, displaying the contoured lower
199 hemisphere projection of the poles to the fault planes (Figure 8b and Figure 9b). MIM results and fault plane
200 distributions are displayed for each individual localities and for fault-slip data covering the entire northern
201 and central domain.

202 ***General stress field and fault population***

203 Figure 8a, 9a show the results of the Multiple Inverse Method applied to the complete fault slip data in these
204 regions. Figure 8b, 9b display plots of the general trend of the fault populations in the northern and in the
205 central domain.

206 The northern domain is dominated by steep dipping fault planes. Three dominant subsets exist, striking
207 approximate NE-SW, E-W and NNW-SSE. The dip varies typically between 90° and 70° , which is consistent
208 with both, normal and strike slip faulting conditions at the time, when the fault planes were initiated. A plot
209 of the MIM results for the complete data set from the N displays three dominant clusters. These clusters
210 indicate two N-S directed tensile events with normal slip conditions and a different event with E-W directed
211 reverse slip, indicating E-W compression (Figure 8a).

212 The variability of recorded stress fields is less pronounced in the central Rwenzoris, compared to the N.
213 Despite the signs for multiple distinct events, only two clearly defined states of stress exist. One dominant
214 event consists of a N-S directed extension under normal slip conditions, other events show roughly NE-SW
215 directed extension combined with SE-NW directed compression, indicating strike-slip to reverse slip
216 conditions.

217 ***Temporal variation of stress inversion results***

218 The heterogeneity of the fault population from single outcrop locations is exemplarily demonstrated in Figure
219 7a, where a lower hemisphere plot of P, B and T axes derived from the planes of the fault population at
220 outcrop BF6 in the N domain is shown. It is evident, that any attempt to determine clusters can be
221 speculative at best. This is a clear sign, that stress field rotation occurred syn-tectonically, resulting in a broad
222 scatter of the results.

223 The degree by which local outcrops have been affected by stress field rotation can be demonstrated if the
224 results of the PBT method are directly compared to results of the DI Method, given that a subgroup of the
225 recorded fault planes and fault lineations mirror distinct singular, but different events. This was possible in
226 case of a subset of the fault-slip data from location BF3 (PBT results of the total fault population is shown in

227 Figure 7a, right, and results of the subset in Figure 7b, left). Results of the Direct Inversion method, applied
228 to the same subset, are shown in Figure 7b, right.

229 A comparison of the mean vectors from the PBT analysis with the principal stress resulting from the Direct
230 Inversion yields the angular distance θ . For the angle between the P-axis and the σ_1 -axis results $\theta = 31^\circ$,
231 for the T-axis and the σ_3 -axis results $\theta = 32^\circ$. The deviation of single results from the mean vector of the
232 P-, B- and T-axis is between 1 % and 4 %, the deviation in case of the DI method is 3° at maximum.

233 This rotation of more than 30° indicates the presence of at least two independent events, where the later one
234 reactivated and overprinted existing fault planes. While the stress derived from fault plane orientation
235 indicates normal faulting and tensile conditions, the later event, derived from the lineation, indicates reverse
236 faulting and compression.

237 ***Spatial variation of stress inversion results***

238 Stress fields calculated from fault-slip data of the northern domain are significantly different from those
239 calculated from stress inversion results of the central domain. The spatial heterogeneity of calculated stress
240 poles is larger in the northern Rwenzoris, compared to the central Rwenzoris (compare Figure 8 and Figure
241 9). Also the orientation of fault planes differs significantly between individual outcrops in the northern
242 domain (Figure 8b and Figure 9b), more so than in the center. For this reason, results for the northern and for
243 the central domain are presented separately.

244 ***Northern domain***

245 Figure 8a displays the results of the Multiple Inverse Method for different locations in the N. Strong
246 variations in the stress inversion results indicate the variability of local stress fields, both temporal and
247 spatial. No distinct first order signals, caused by the continental extension, dominates the stress inversion
248 results in the sense of a single repeating signal, which occurs over all domains.

249 Two possible exceptions from this rule are cluster A at localities BF1-BF3, which is similar to cluster A at
250 locality BF5-BF6, and cluster A at locality BF4, which resembles cluster B at locality BF5. These clusters
251 indicate ENE-WSW and ESE-WNW extension, respectively, for outcrops BF1 to BF4, located in the N. The

252 extent of the clusters indicates a transition of the general stress state between normal faulting and strike slip
253 faulting.

254 It is, however, possible to identify a general trend in the local stress inversion results. This trend indicates a
255 transition of the stress regime from the northern-most outcrops, where a rift graben has been formed, to the
256 localities further south, where the Rwenzori block is still attached to the Victoria plate.

257 Strike and dip of fault planes (Figure 8b) varies significantly between the localities, just as the results of the
258 stress inversion. The stress inversion results are usually not compatible with the fault plane orientation,
259 which indicates a major reactivation of existing planes including inversion of the stress field. This is
260 consistent with field observations of reverse slip indicators. The general orientation of fault planes is
261 indicated by a dominance of N-S to NNE-SSW striking fault planes with steep to intermediate dip to the E.

262 The orientation of the σ_1 poles at outcrops in the very S of the northern domain, at locations BF7 and BF8,
263 indicates ESE-WNW compression. Tensile polyphase stress is oriented at NNE-SSW and vertical,
264 respectively. Thus, the general stress state varies between strike slip and compressive reverse faulting
265 conditions.

266 Outcrops BF5 and BF 6 are located at the intersection of the main boundary faults in the NE, and mark the
267 transition between the stress regimes in the S and the N of the profile. The tensile stress in these outcrops
268 varies spans the whole range from ESE-WSW to N-E tension. This orientation of the tensile stress is
269 consistent with the adjacent main boundary normal faults, whose sense of displacement is indicated by recent
270 seismic data (Koehn et al. 2010) and the general presence of a graben.

271 Figure 8 includes MIM results based on the entire data set from the N, using the complete data set of
272 outcrops BF1 to BF8. This larger data set can help to identify the most dominant recorded stress fields for the
273 whole area, instead just single outcrops. Here, the clearest signals indicate two NNE-SSW directed tensile
274 events with normal faulting (with vertical) and an event with ESE-WNW directed compression and reverse
275 faulting (vertical σ_3 -orientation).

276 **Central Rwenzoris**

277 MIM stereo plots based on fault-slip data from Kitandara Hut and from Elena Hut are very similar, with three
278 dominant events indicating approximate SE-NW compression and N-S to SW-NE extension. These events
279 also show similar stress ratios (Figure 9a). A stereoplot of MIM (Figure 9a) generated stress poles from
280 Bujuku Hut displays a very different stress scenario, with three dominant events with ESE-WNW extension
281 associated with normal fault conditions.

282 The stress poles calculated for Elena Hut and for the entire dataset from Elena, Bujuku and Kitandara
283 indicate also minor reverse tectonics, with vertical σ_3 and compression with either N-S or NW-SE
284 orientation (Figure 9a).

285 All locations in the central Rwenzoris show two dominant fault populations: a set of normal fault planes
286 combined with a set of steeply dipping fault planes indicating strike slip. Planes to normal faults strike
287 usually approximately NE-SW, slip indicators on these normal faults indicate late reverse slip.

288 The other dominant element in the central Rwenzoris are steep fault planes, indicating strike slip faulting,
289 typically striking approximate NW-SE. The exception are the surroundings of Bujuku hut, where steep fault
290 planes strike in a NE-SW direction.

291 **Discussion**

292 Brittle faulting in the area may have started as early as the early Phanerozoic, when the Precambrian rocks in
293 the Rwenzori area were exhumed above the 300° C isotherm (Bauer et al., 2010), but, fault slip caused by
294 recent, Cenozoic rifting of the Nubia-Somalia plate boundary overprints existing structures. This assumption
295 is supported by the typical mismatch between the stress indicated by the orientation of fault planes and stress
296 calculated from slip indicators on the fault planes. Heterogeneity of calculated stresses, both in space and
297 time, hint at crustal deformation associated with rifting and block capture that is consistent with numerical
298 modeling of these processes (Koehn et al., 2010). Associated syntectonic changes of local stress fields are
299 also consistent with this hypothesis as shown by Sachau et al. (2011) in a numerical model.

300 The variation in local stress fields detected in this work may be related to crustal deformation from past,

301 present, or overprinting of present-day tectonics on existing structures (Corti, 2011). Kinematic movements
302 possibly affecting the local stress fields include (i) rotation of the first-order stress field (ii) new border fault
303 creation to the NE and east of the Rwenzori, (iii) active rotation of the Rwenzori microplate relative to the
304 diverging Nubian and Victoria plates, or (iv) rotation of internal blocks from segmentation of the Rwenzoris

305 (i) The amount of rotation of the first-order stress field in the Western Branch of the EARS is still under
306 debate. however, stress reorientation at the order of up to $7.5^{\circ}/10^5$ years has been suggested for East Africa
307 (Bosworth et al., 1992) and may have occurred in this region. Stress reorientation acting on, or creating, the
308 complex geometry of the rift in the northwestern Rwenzori region could explain strong heterogeneities in the
309 local stress field there. In this region two major rift faults with different strike intersect (Figure 2 and Figure
310 3). The major border fault strikes NNE-SSW dipping ESE, while the other major fault strikes ENE-WSE,
311 dipping to the N.

312 (ii) Active rifts that overprint existing heterogeneities can develop new border faults along zones of
313 weaknesses (Van Wijk, 2005). New seismic studies suggest regions of melt intrusions in the crust east of the
314 Rwenzori and north of the Rwenzori (Lindenfield et al., 2012) where we find significant variations in the
315 local stress field. Active magmatism can weaken the lithosphere (Buck, 2006) allowing for rupture to occur
316 in regions without large boundary forces, i.e. from subduction, such that new faults will develop. The
317 complex local stress field in the NE of the Rwenzori is consistent with new border fault creation here such
318 that the horst will become detached from the Victoria block.

319 (iii) The strong variability of the stress field in the northern Rwenzoris and relatively less heterogeneous
320 stress fields in the central Rwenzoris can be explained by rotation of the Rwenzori block with respect to the
321 Nubian and Victoria plates. The anti-clockwise rotation of the Victoria plate with respect to the Nubian plate
322 results in transtension relative to the Rwenzori microplate, which may be exacerbated if the Rwenzori are
323 actively rotating clockwise. Transtension, which includes both, normal slip and strike slip events, can explain
324 the wide scatter of stress poles in the stereoplot for individual events. Even clusters, which can be attributed
325 to single events (for instance at locality BF1 (Figure 8a)), span typically the range between strike slip and
326 normal or reverse slip conditions. Outcrops with clearly distinguishable events show the same pattern of
327 alternating pure shear and simple shear conditions (outcrops BF5 to BF8 in Figure 8a).

328 The dominance of generally steep fault planes in the N can be explained by oblique divergence of the Nubian
329 and Victoria plate. Present-day steep faults are pre-existing structures that accommodate strain, in part, with
330 simple shear component. These pre-existing fault planes accommodated pure shear in the past when pure
331 normal and reverse slip occurred, thus several faulting events are overprinted by present-day slip indicators.
332 The large number of individual events found in our stress inversions are indicative of strain partitioning,
333 where two different stress regimes have to be accommodated.

334 In the southern localities of the northern domain, where the Rwenzori block is still attached to the Victoria
335 plate, fault inversion with local horizontal shortening occurs. This can be explained rotation of the Rwenzori
336 block relative to the surrounding plates such that compression occurs in the NE. Localities at more northward
337 positions, where the Rwenzori plate is already detached from the Victoria plate and a rift graben has formed,
338 do not show any signs of a major compression. This may suggest that compression occurred only after the
339 rift formation.

340 Recent seismic data (Lindenfeld et al. 2012) have shown, that the sense of the major fault in vicinity of the
341 outcrop locations in the N is presently normal with a sinistral component. This indicates approximately ESE
342 tension, parallel to the general translation vector of the Victoria plate.

343 The spatial variation of calculated stress poles is less pronounced in the central Rwenzori when compared to
344 the north (Figure 8a and Figure 9a), which is not surprising since the area is located in the interior of the
345 Rwenzori microplate. , Thus the central Rwenzori are not affected by plate-plate interactions.

346 (iv) It has been proposed that the central Rwenzoris have been segmented into internal blocks by transection
347 faults, each with its own kinematics and its own local stress field (e.g. Ring 2008; Bauer et al., 2014). The
348 lineament map (Figure 10) suggests that the sample localities at Kitandara and Elena Hut are on the same
349 block while Bujuku is on a different block. A multiple block model can explain that the calculated stress
350 field for Elena and Bujuku are distinctly different despite their geographic proximity. The same argument
351 applies the similarity of calculated stress poles for data from Elena and Kitandara, however it is difficult to
352 distinguish between present-day and paleo-stress fields in the central Rwenzori where geodetic observations
353 of surface motions are needed to test an actively segmenting Rwenzori block model.

354 **Conclusion**

355 Fault-slip data from the northern Rwenzori show an unusually large heterogeneity, both in space and time,
356 compared to other studies applying stress inversion. Individual localities in the northern domain experience
357 polyphase tectonics, probably due to transpression tectonics of the Victoria plate and the Rwenzori
358 microplate. Each phase of tectonic stress affects the local fault population, leading to heterogeneous fault-slip
359 data. Faults show strong overprinting relationships and the stress field that initiated the fault plane is usually
360 not the same that created the slip indicators.

361 Fault-slip data from the central Rwenzori are more homogeneous compared to stress fields along the borders
362 of the microplate. The results of the fault inversion in that domain, in conjunction with the visible
363 lineaments, may indicate independent stress fields for multiple blocks in the central Rwenzori area.

364 **References**

- 365 Angelier, Jacques. 1990. "Inversion of Field Data in Fault Tectonics to Obtain the Regional stress—III. A
366 New Rapid Direct Inversion Method by Analytical Means." *Geophysical Journal International* 103:
367 363–376.
- 368 Bahat, Dov, and Mohr, Paul. 1987. "Horst Faulting in Continental Rifts." *Tectonophysics* 141 (1-3): 61–73.
369 doi:10.1016/0040-1951(87)90174-0.
- 370 Bauer, F. U., Glasmacher, U. A., Ring, U., Schumann, A., & Nagudi, B. 2010. "Thermal and exhumation
371 history of the central Rwenzori Mountains, Western Rift of the East African Rift System, Uganda".
372 *International Journal of Earth Sciences* 99:1575-1597.
- 373 Bauer, F. U., Glasmacher, U. A., Ring, U., Karl, M., Schumann, A., Nagudi, B. 2013. "Tracing the
374 exhumation history of the Rwenzori Mountains, Albertine Rift, Uganda, using low-temperature
375 thermochronology", *Tectonophysics* 599: 8-28, doi:10.1016/j.tecto.2013.03.032.
- 376 Bosworth, William, Strecker, M. R., and Blisniuk, P. M.. 1992. "Integration of East African Paleostress and
377 Present-Day Stress Data: Implications for Continental Stress Field Dynamics." *Journal of Geophysical*
378 *Research* 97 (B8): 11851. doi:10.1029/90JB02568.
- 379 Delvaux, D., Kervyn, A., Macheyeke, A. S. and Temu, E.B. 2012. "Geodynamic significance of the TRM
380 segment in the East African Rift (W-Tanzania): Active tectonics and paleostress in the Ufipa plateau
381 and Rukwa basin". *Journal of Structural Geology* 37: 161-180.
- 382 Delvaux, D., & Barth, A. 2010. "African stress pattern from formal inversion of focal mechanism data".
383 *Tectonophysics* 482:105-128.
- 384 Ebinger, C. J. 1989. "Tectonic Development of the Western Branch of the East African Rift System."
385 *Geological Society of America Bulletin* 101: 885–903.
- 386 Fernandes, R. M. S., Miranda, J. M., Delvaux, D., Stamps, D. S., Saria, E. 2013. "Re-evaluation of the
387 kinematics of Victoria Block using continuous GNSS data." *Geophysical Journal International* 193:1-
388 10. doi: 10.1093/gji/ggs071.

- 389 Foster, Adrian, and Francis Nimmo. 1996. "Comparisons Between the Rift Systems of East Africa, Earth and
390 Beta Regio, Venus." *Earth and Planetary Science Letters* 143 (1-4) (September): 183–195.
391 doi:10.1016/0012-821X(96)00146-X.
- 392 Homberg, C., J. C. Hu, J. Angelier, F. Bergerat, and O. Lacombe. 1996. "Characterization of Stress
393 Perturbations Near Major Fault Zones: Insights from 2-D Distinct-Element Numerical Modelling and
394 Field Studies (Jura Mountains)." *Journal of Structural Geology* 19: 703–718.
- 395 Karner, G D, B R Byamungu, C J Ebinger, A B Kampunzu, R K Mukasa, J Nyakaana, and N M Upcott.
396 2000. "Distribution of Crustal Extension and Regional Basin Architecture of the Albertine Rift System,
397 East Africa." *Marine and Petroleum Geology* 17 (March 1864): 1131–1150.
- 398 Koehn, D., K. Aanyu, S. Haines, and T. Sachau. 2008. "Rift Nucleation, Rift Propagation and the Creation of
399 Basement Micro-Plates Within Active Rifts." *Tectonophysics* 458 (1-4) (October 15): 105–116.
400 doi:10.1016/j.tecto.2007.10.003.
- 401 Koehn, D., M. Lindenfeld, G. Rumpker, K. Aanyu, S. Haines, C. W. Passchier, and T. Sachau. 2010. "Active
402 Transsection Faults in Rift Transfer Zones: Evidence for Complex Stress Fields and Implications for
403 Crustal Fragmentation Processes in the Western Branch of the East African Rift." *International Journal
404 of Earth Sciences* 99 (7) (March 17): 1633–1642. doi:10.1007/s00531-010-0525-2.
- 405 Lindenfeld, M., Rumpker, G., Batte, A., and Schumann, A. "Seismicity from February 2006 to September
406 2007 at the Rwenzori Mountains, East African Rift: earthquake distribution, magnitudes and source
407 mechanisms." *Solid Earth Discussion* 4(1): 251-264.
- 408 Lindenfeld, M., Rumpker G., Link, K., Koehn, D., and Batte, A.. 2012. "Fluid-Triggered Earthquake Swarms
409 in the Rwenzori Region, East African Rift—Evidence for Rift Initiation." *Tectonophysics* 566-567
410 (September): 95–104. doi:10.1016/j.tecto.2012.07.010.
- 411 Link, K., Koehn, D., Barth, M., Tiberindwa, J., Barifaijo, E., Aanyu, K. and Foley, S.. 2010. "Continuous
412 Cratonic Crust Between the Congo and Tanzania Blocks in Western Uganda." *International Journal of
413 Earth Sciences* 99 (7) (June 2): 1559–1573. doi:10.1007/s00531-010-0548-8.
- 414 Macdonald, Ken C., Daniel S. Scheirer, and Suzanne M. Carbotte. 1991. "Mid-Ocean Ridges:

- 415 Discontinuities, Segments and Giant Cracks.” *Science* 253 (5023): 986–994.
416 doi:10.1126/science.253.5023.986.
- 417 Morley, CK, and RA Nelson. 1990. “Transfer Zones in the East African Rift System and Their Relevance to
418 Hydrocarbon Exploration in Rifts (1).” *AAPG Bulletin* 74: 1234–1253.
- 419 Moustafa, Adel R. 1997. “Controls on the Development and Evolution of Transfer Zones: The Influence of
420 Basement Structure and Sedimentary Thickness in the Suez Rift and Red Sea.” *Journal of Structural
421 Geology* 19 (6) (June): 755–768. doi:10.1016/S0191-8141(97)00007-2.
- 422 Osmaston, H. 1989. “Glaciers, Glaciations and Equilibrium Line Altitudes on the Rwenzori.” In *Quaternary
423 and Environmental Research on East African Mountains*, edited by W. G. Mahaney, 31–104.
424 Rotterdam: Balkema.
- 425 Otsubo, Makoto, and Atsushi Yamaji. 2006. “Improved Resolution of the Multiple Inverse Method by
426 Eliminating Erroneous Solutions.” *Computers & Geosciences* 32 (8) (October): 1221–1227.
427 doi:10.1016/j.cageo.2005.10.022.
- 428 Pollard, D. D., S. D. Saltzer, and A. M. Rubin. 1993. “Stress Inversion Methods: Are They Based on Faulty
429 Assumptions?” *Journal of Structural Geology* 15: 1045–1054.
- 430 Reiter, F., and P. Acs. 2003. “TectonicsFP — a Computer Program for Structural Geology.”
- 431 Ring, Uwe. 2008. “Extreme Uplift of the Rwenzori Mountains in the East African Rift, Uganda: Structural
432 Framework and Possible Role of Glaciations.” *Tectonics* 27 (4) (August 27): TC4018.
433 doi:10.1029/2007TC002176.
- 434 Sachau, Till, and Daniel Koehn. 2010. “Faulting of the Lithosphere During Extension and Related Rift-Flank
435 Uplift: a Numerical Study.” *International Journal of Earth Sciences* 99 (7): 1619–1632.
436 doi:10.1007/s00531-010-0513-6.
- 437 Sachau, Till, Daniel Koehn, and Cees Passchier. 2011. “Lattice-Particle Simulation of Stress Patterns in a
438 Rwenzori-Type Rift Transfer Zone.” *Journal of African Earth Sciences* 61 (4) (November): 286–295.
439 doi:10.1016/j.jafrearsci.2011.08.006.

- 440 Saria, E., Calais, E., Stamps, D. S., Delvaux, D. and Hartnady, C. J. H. 2014. "Present-day kinematics of the
441 East African Rift." *Journal of Geophysical Research* 119: 3584-3600. doi: 10.1002/2013JB010901.
- 442 Shan, Yehua, Zian Li, and Ge Lin. 2004. "A Stress Inversion Procedure for Automatic Recognition of
443 Polyphase Fault/slip Data Sets." *Journal of Structural Geology* 26 (5) (May): 919–925.
444 doi:10.1016/j.jsg.2003.10.001.
- 445 Sippel, Judith, Magdalena Scheck-Wenderoth, Klaus Reicherter, and Stanislaw Mazur. 2009. "Paleostress
446 States at the South-Western Margin of the Central European Basin System — Application of Fault-Slip
447 Analysis to Unravel a Polyphase Deformation Pattern." *Tectonophysics* 470 (1-2) (May): 129–146.
448 doi:10.1016/j.tecto.2008.04.010.
- 449 Stamps, D. Sarah, Eric Calais, Elifuraha Saria, Chris Hartnady, Jean-Mathieu Nocquet, Cynthia J. Ebinger,
450 and Rui M. Fernandes. 2008. "A Kinematic Model for the East African Rift." *Geophysical Research*
451 *Letters* 35 (5).
- 452 Taylor, R. G., and K. W. F. Howard. 1998. "Post-Palaeozoic Evolution of Weathered Landsurfaces in Uganda
453 by Tectonically Controlled Cycles of Deep Weathering and Stripping." *Geomorphology* 25: 173–192.
- 454 Tikoff, B., and S. F. Wojtal. 1999. "Displacement Control of Geologic Structures." *Journal of Structural*
455 *Geology* 21: 959–967.
- 456 Turner, F.J. 1953. "Nature and Dynamic Interpretation of Deformation Lamellae in Calcite of Three
457 Marbles." *American Journal of Science* 251 (4): 276–298.
- 458 Upcott, N. M., R. K. Mukasa, C. J. Ebinger, and G. D. Karner. 1996. "Along-Axis Segmentation and Isostasy
459 in the Western Rift, East Africa." *Journal of Geophysical Research* 101 (B2): 3247.
460 doi:10.1029/95JB01480.
- 461 Van Wijk, J. W. 2005. "Role of weak zone orientation in continental lithosphere extension". *Geophysical*
462 *Research Letters* 32(2).
- 463 Yamaji, Atsushi. 2000. "Multiple Inverse Method: a New Technique to Separate Stresses from
464 Heterogeneous Fault-Slip Data." *Journal of Structural Geology* 22: 441–452.

465 **Figure captions**

466 **Figure 1:**

467 Simplified geographical and geological overview map of the Rwenzori area (adapted from Link et al. 2010)□.
468 Gray units represent gneisses of the Gneissic Granulite Complex and sandstones, conglomerates and
469 argillaceous sediments of the Kibaran Belt. Green units represent the Buganda-Toro Belt, consisting mainly
470 of schists, amphibolites, quartzites. Thick black lines mark major boundary faults of the rifts and the
471 Rwenzori horst.

472 **Figure 2:**

473 Tectonic map of the Rwenzori area and 19 fault plane solutions of seismic events around the Rwenzori
474 micro-plate. Fault plane solutions show compressional quadrants in red and extensional quadrants in white.
475 Black symbols in the interior of the Rwenzoris mark the approx. location of the dominating brittle fault
476 systems. The fault plane solutions illustrate the heterogeneity of the local present-day stress field.

477 **Figure 3:**

478 a) Plate movements of the Rwenzori micro-plate and the Victoria plate, with fixed Nubia plate. Marked is the
479 proposed center of rotation of the Rwenzori block and the translation of the Victoria plate. b) Proposed stages
480 of the Rwenzori development ((Koehn et al. 2008)□). Stage I: initial development; stage II: block rotation;
481 stage III: capturing and detachment.

482 **Figure 4:**

483 Photographs of brittle faults typical for the Rwenzori area. a) Fault plane with lineation in amphibolite in the
484 central Rwenzoris. b) Flower structure in young volcanic ash near Lake Edwards.

485 **Figure**

5:

486 Sample locations in the northern Rwenzoris and in the central Rwenzoris. Red dots are sample locations,
487 green dots are orientation points. The data come from two different domains, marked by the rectangles,
488 which are referred to as the northern domain and the central domain in the text.

489 **Figure 6:**

490 Hoeppener plots of the fault slip data, which are used for stress inversion. The localities are indicated
491 according to Figure 5. Fault planes are indicated by their corresponding poles in lower hemisphere
492 projection. Fault plane lineations are drawn into the pole points. Arrow heads indicate the sense of movement
493 of the hanging wall block.

494 **Figure 7:**

495 Stress inversion results visualizing the heterogeneity and the rotation of the recorded stress field. a)
496 Stereoplots display results of the PBT method, which calculates stress from the orientation of single fault
497 planes, for outcrops BF6 and BF3 in the northern Rwenzoris. The BF6 data is more heterogeneous than BF3,
498 which is the least heterogeneous data set in this study. b) Stereoplot of a homogeneous subset in the BF3
499 data. The results from PBT and the results from DIM differ by 30°, both with very small error margins. See
500 text for further explanation.

501 **Figure 8:**

502 Results of the MIM calculations and fault plane distribution for data from the northern domain, shown in
503 lower hemisphere stereoplots. Green dots: landmarks, red dots: sample locations. a) Results of MIM
504 calculations for datasets from individual outcrops or combinations of adjacent outcrops. Bottom left is a plot
505 of MIM results for the combined data set of all outcrops. Colors indicate Φ values, violet and red are
506 uniaxial states of stress. b) Contour plots of poles to fault planes, for the same datasets as in a.

507 **Figure 9:**

508 Results of the MIM calculations and fault plane distribution for data from the central and the eastern
509 Rwenzoris, shown in lower hemisphere stereoplots. The further description is identical to Figure 8.

510 **Figure 10:**

511 Lineament map of the central Rwenzoris. Lineaments are linear features in the landscape.

Figure 1

[Click here to download Figure: Fig_1.eps](#)

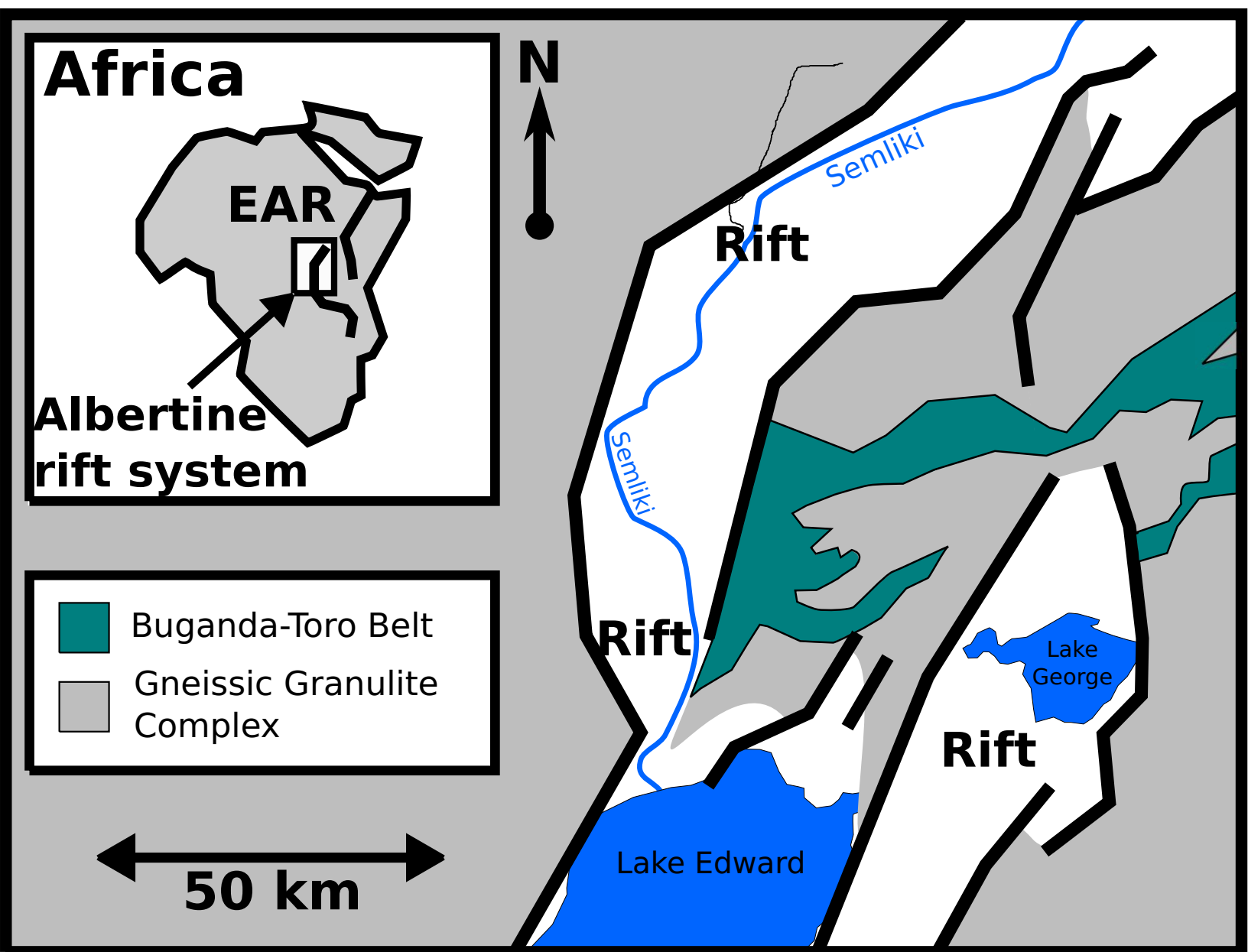
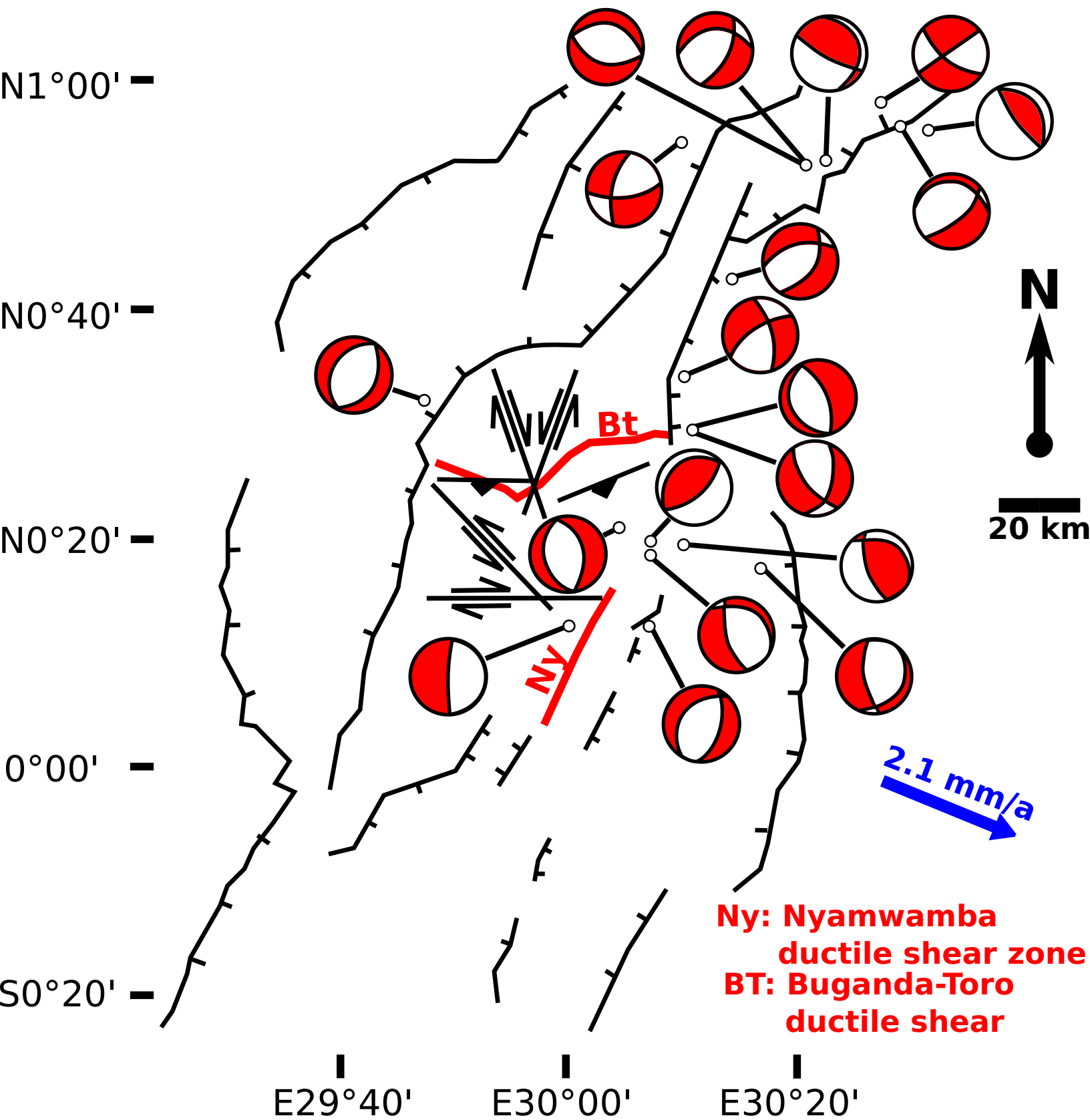


Figure 2

[Click here to download Figure: Fig 2.eps](#)



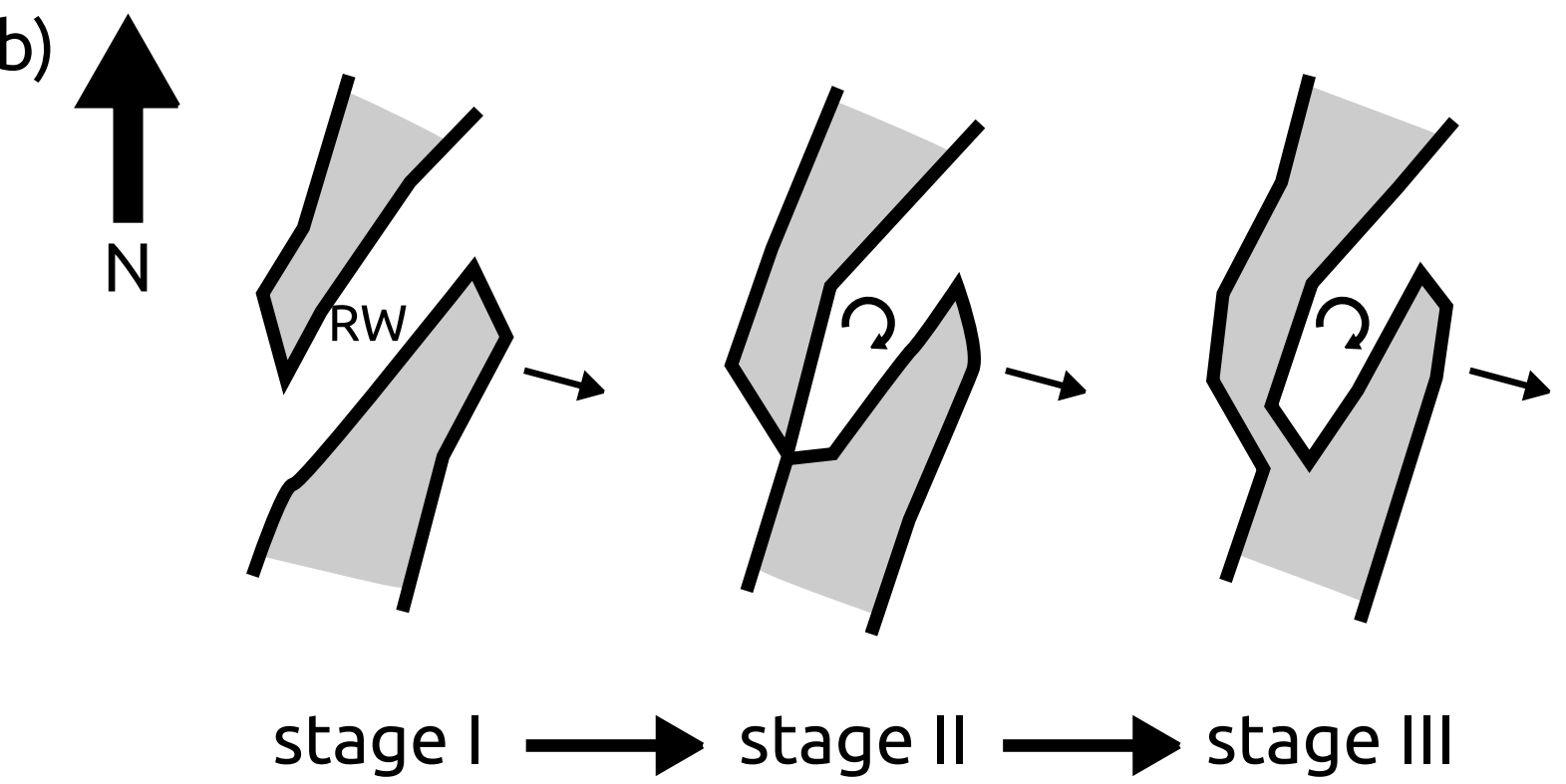
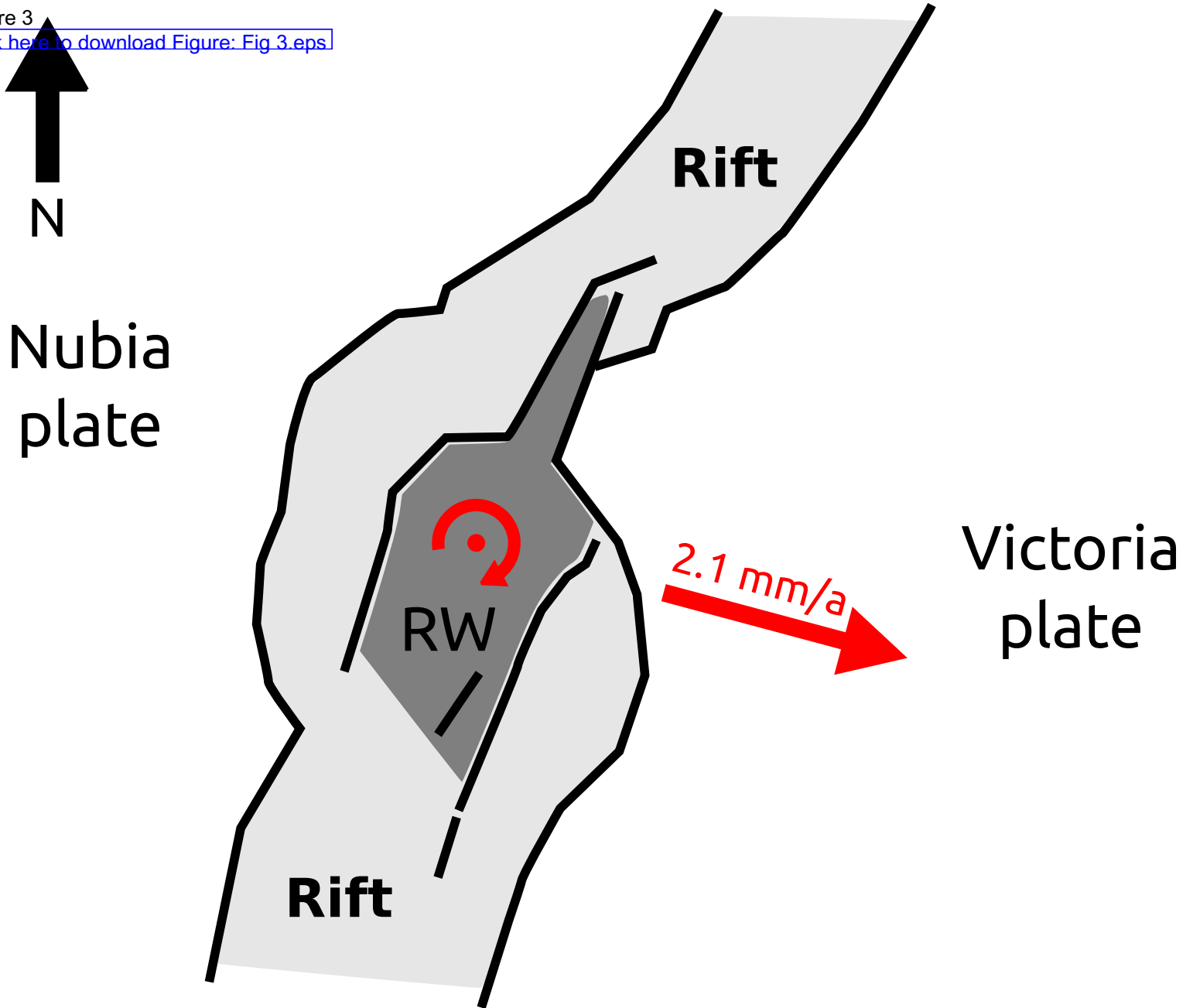


Figure 4

[Click here to download Figure: Fig 4.eps](#)

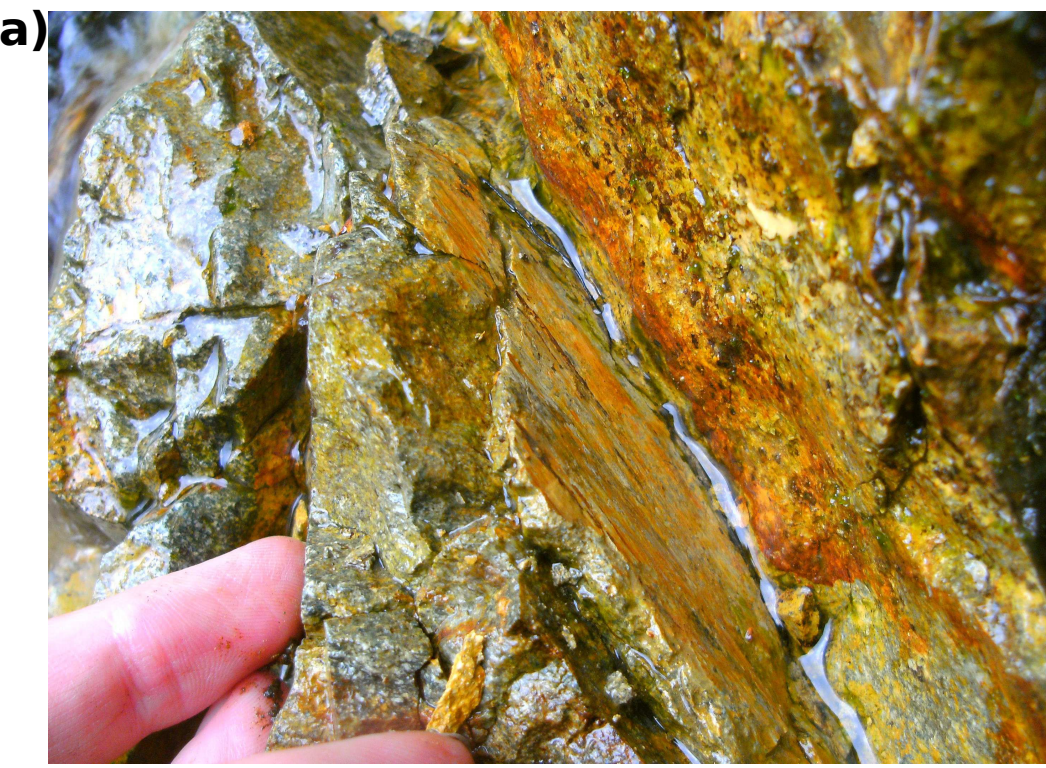


Figure 5

[Click here to download Figure: Fig.5.eps.](#)

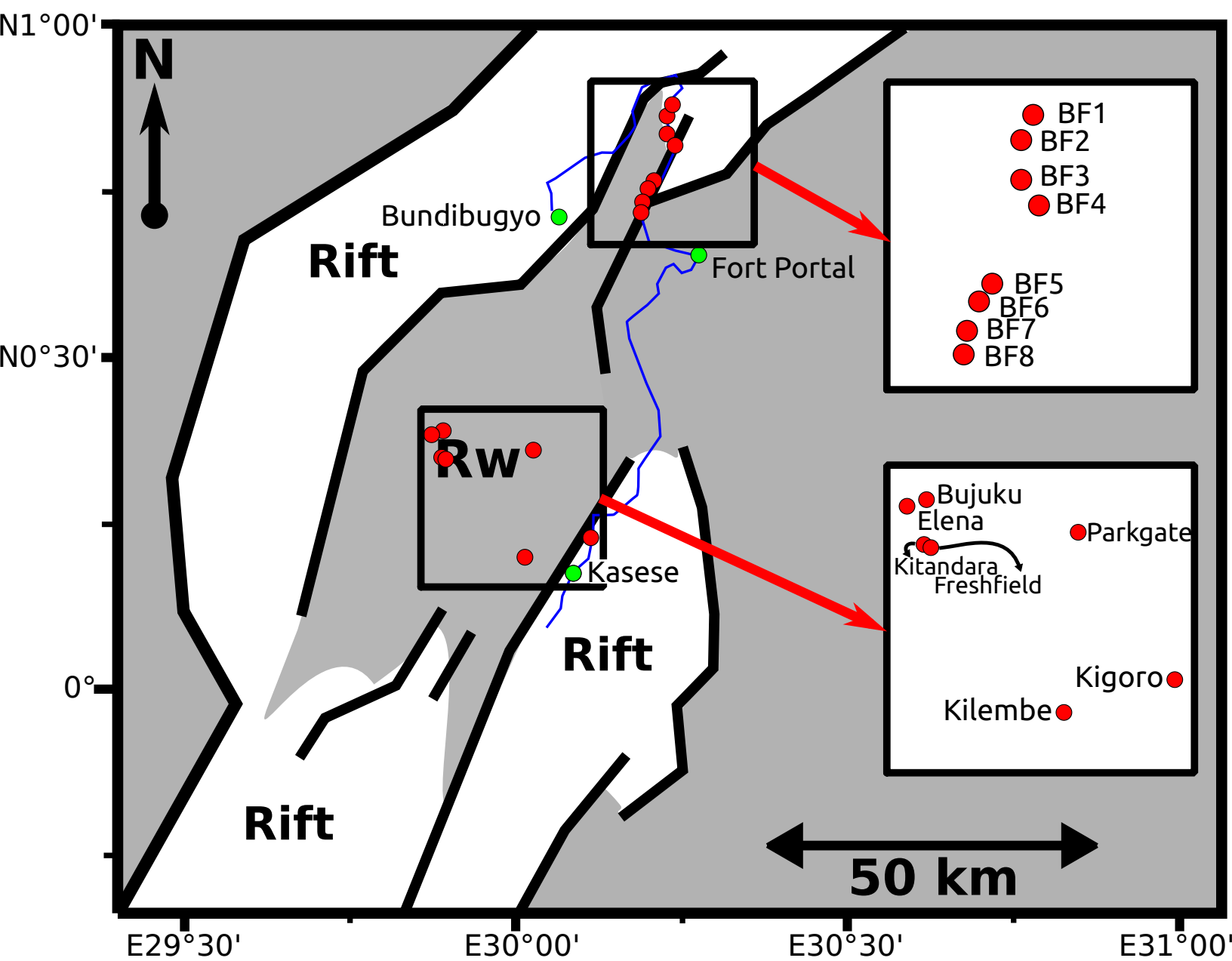
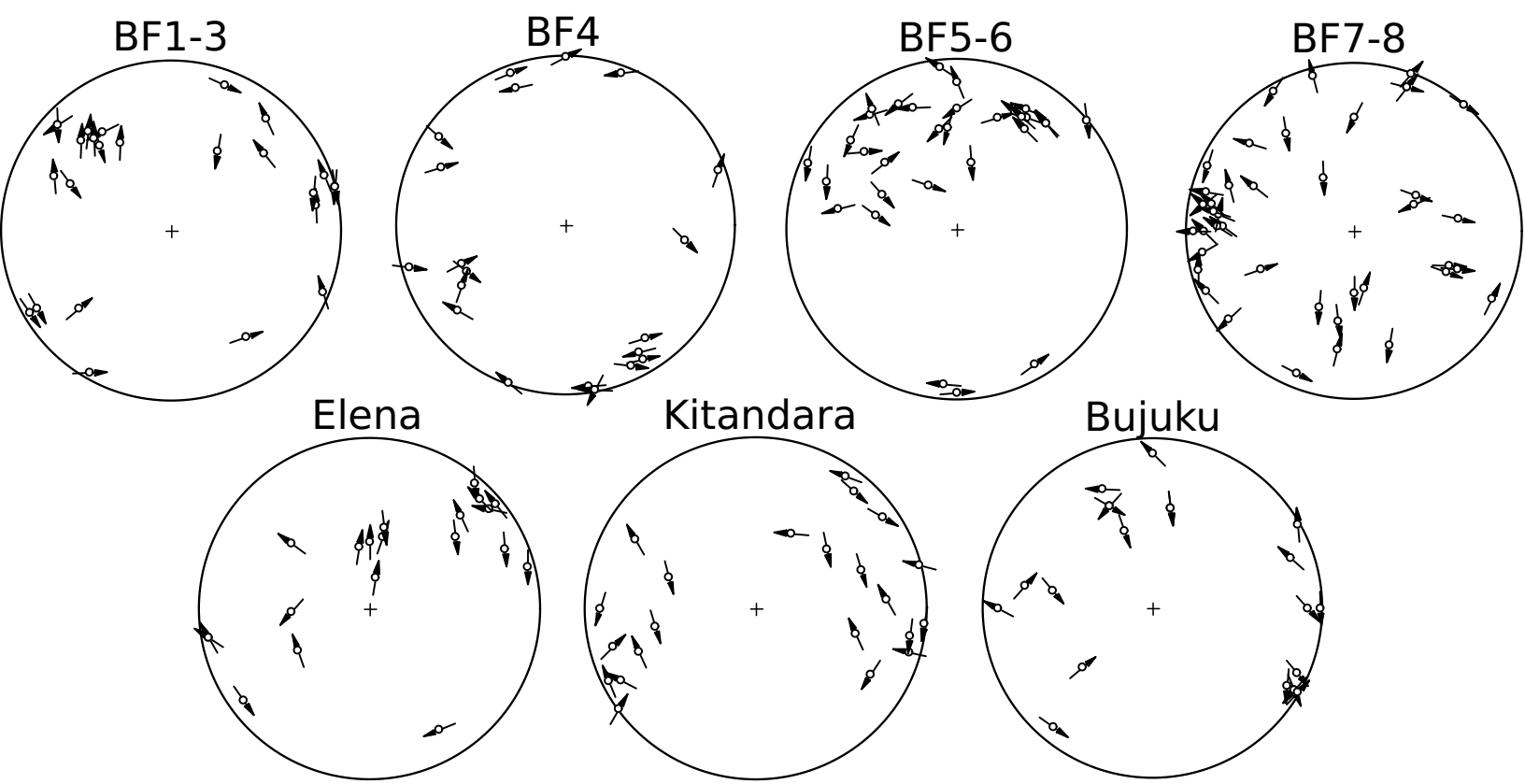
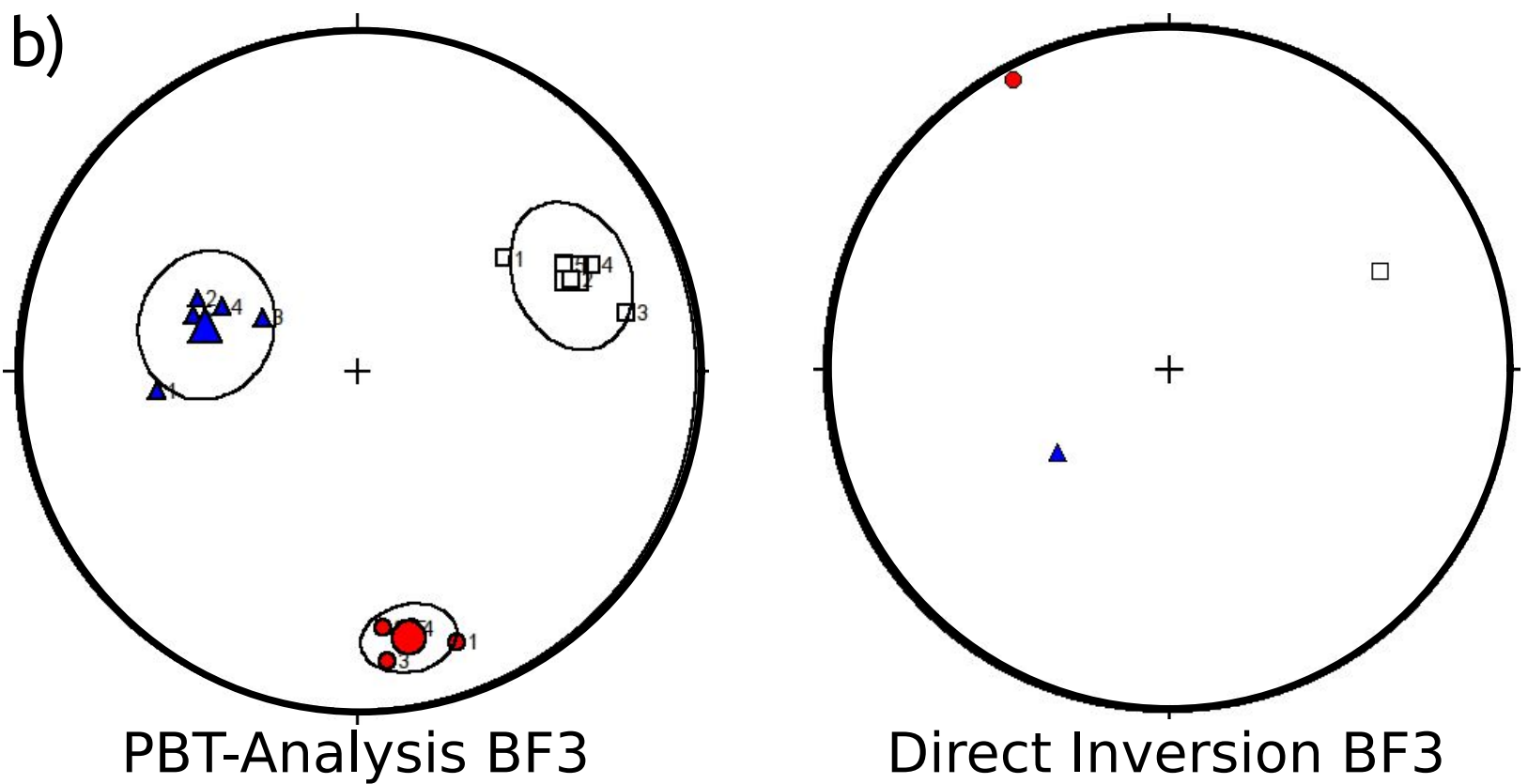
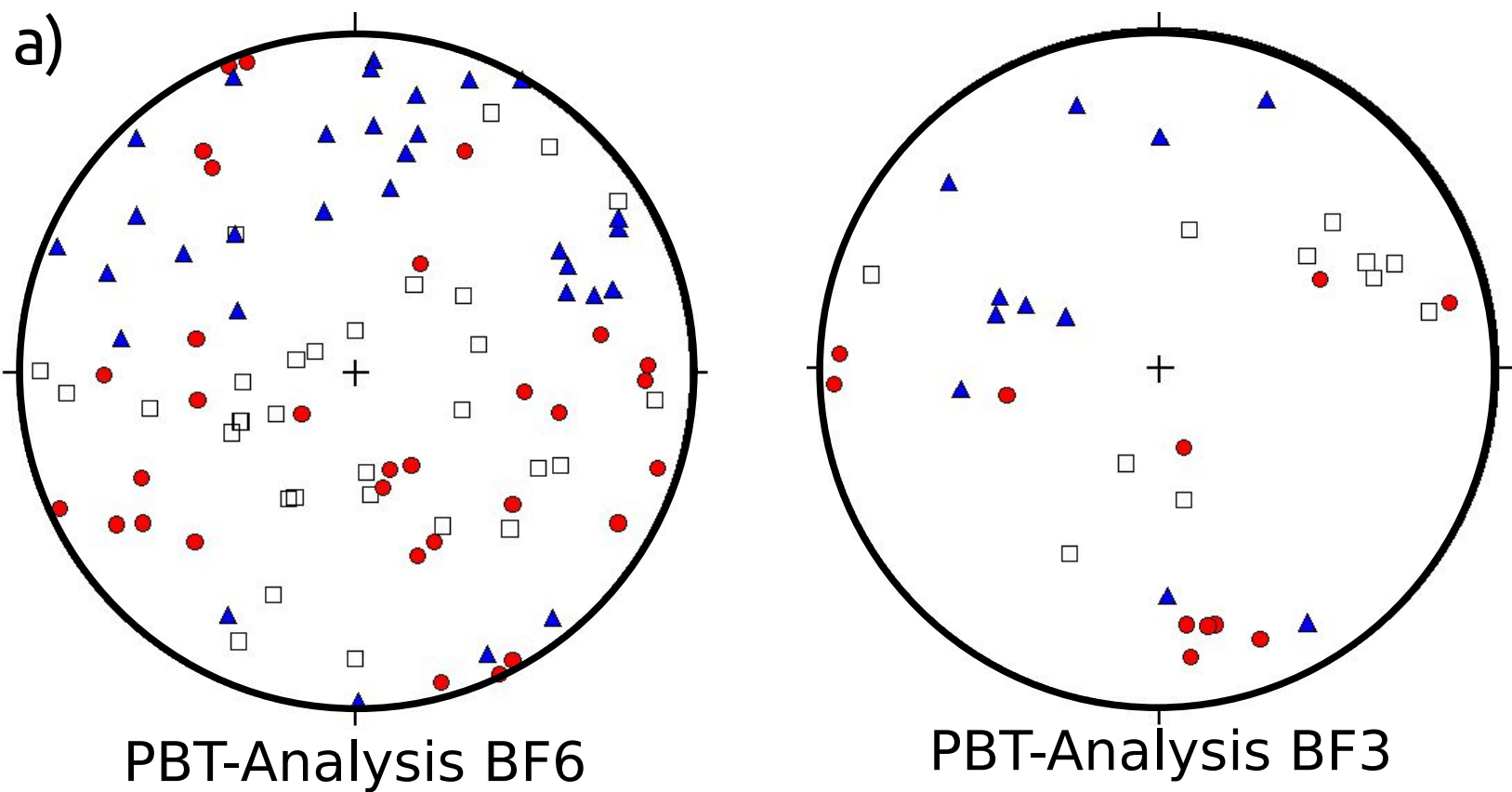


Figure 6

[Click here to download Figure: Fig 6.eps](#)

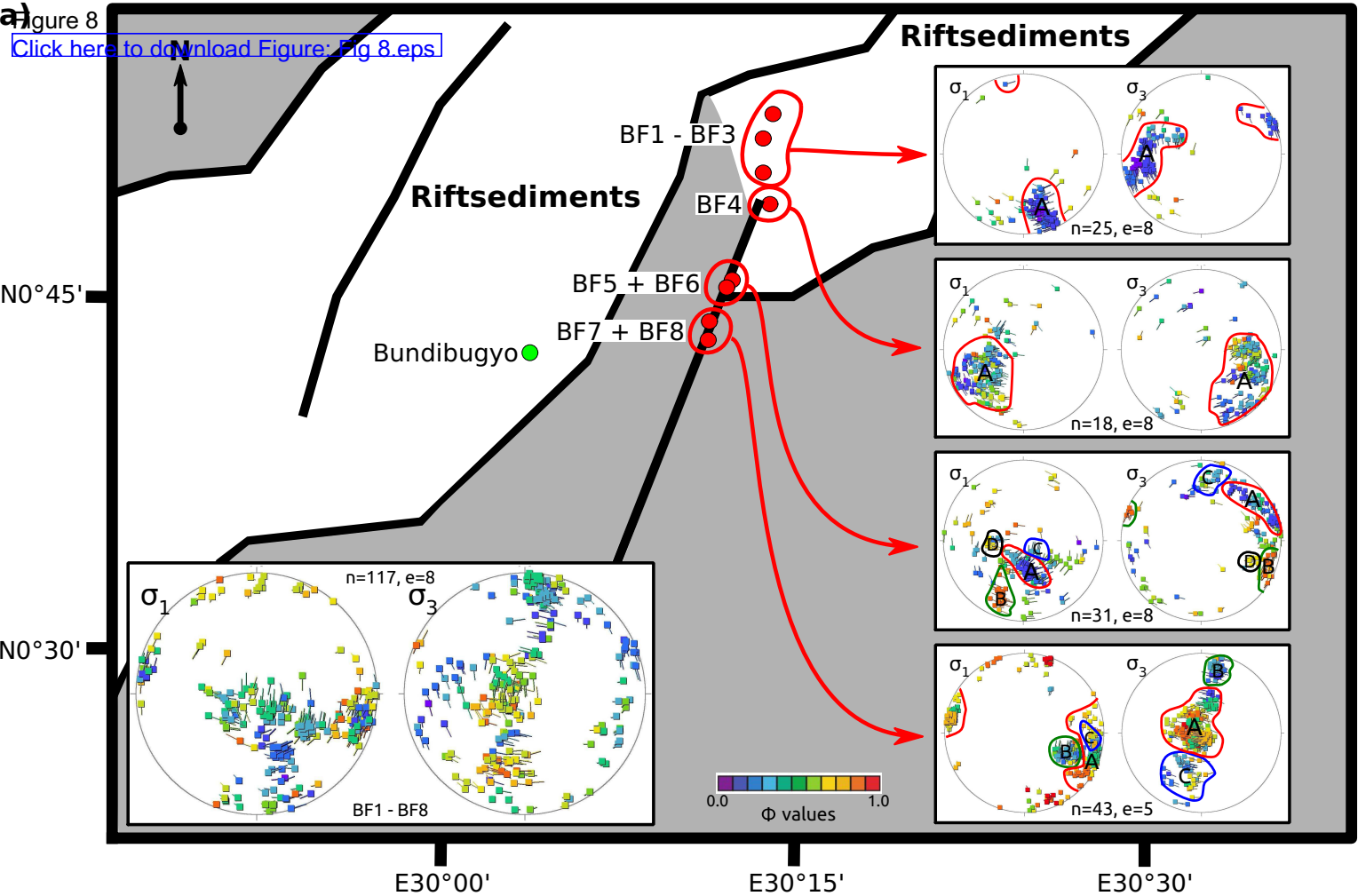




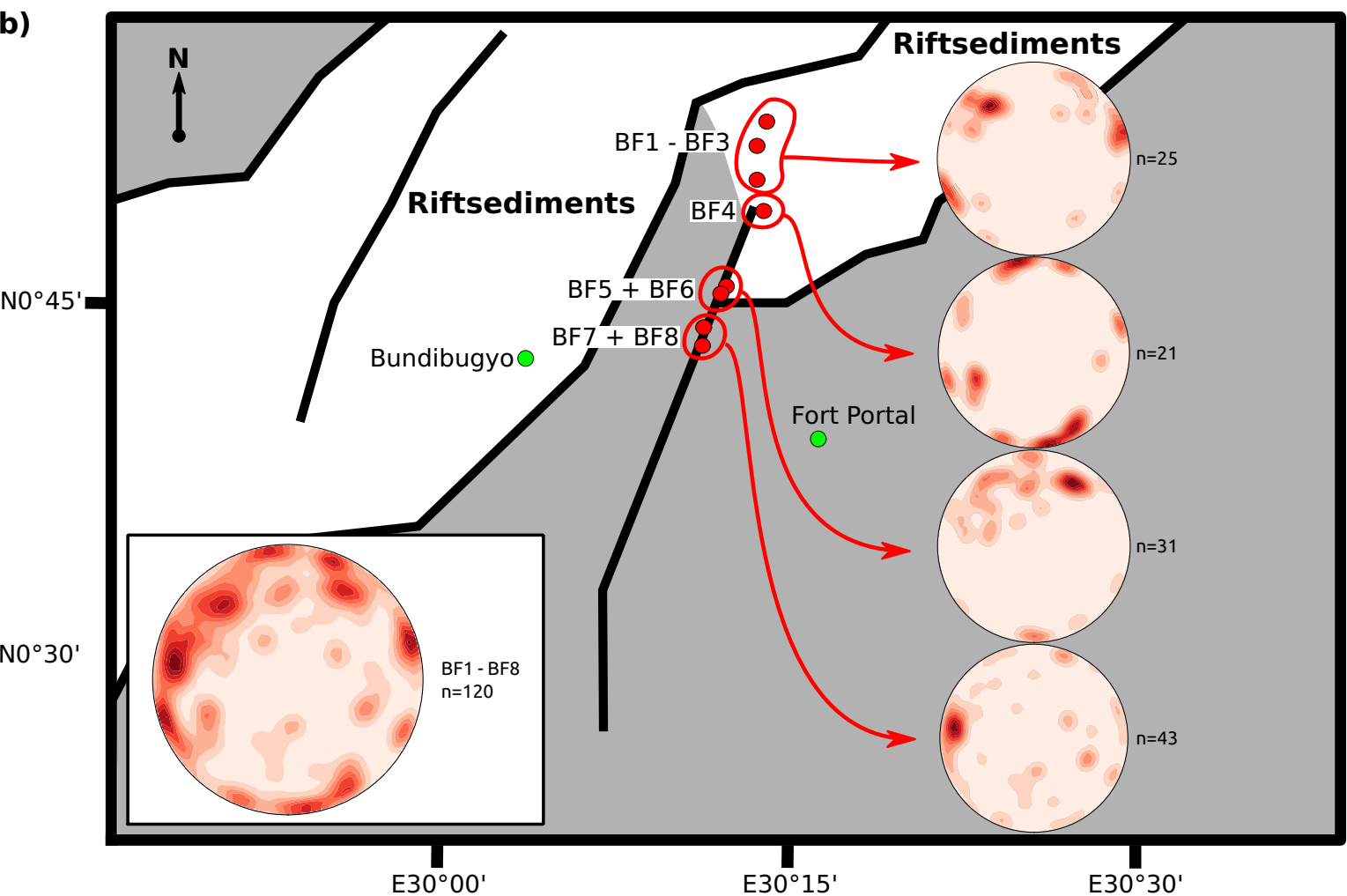
P (compression): ● B (neutral): □ T (tension): ▲

a) Figure 8

[Click here to download Figure: Fig 8.eps](#)

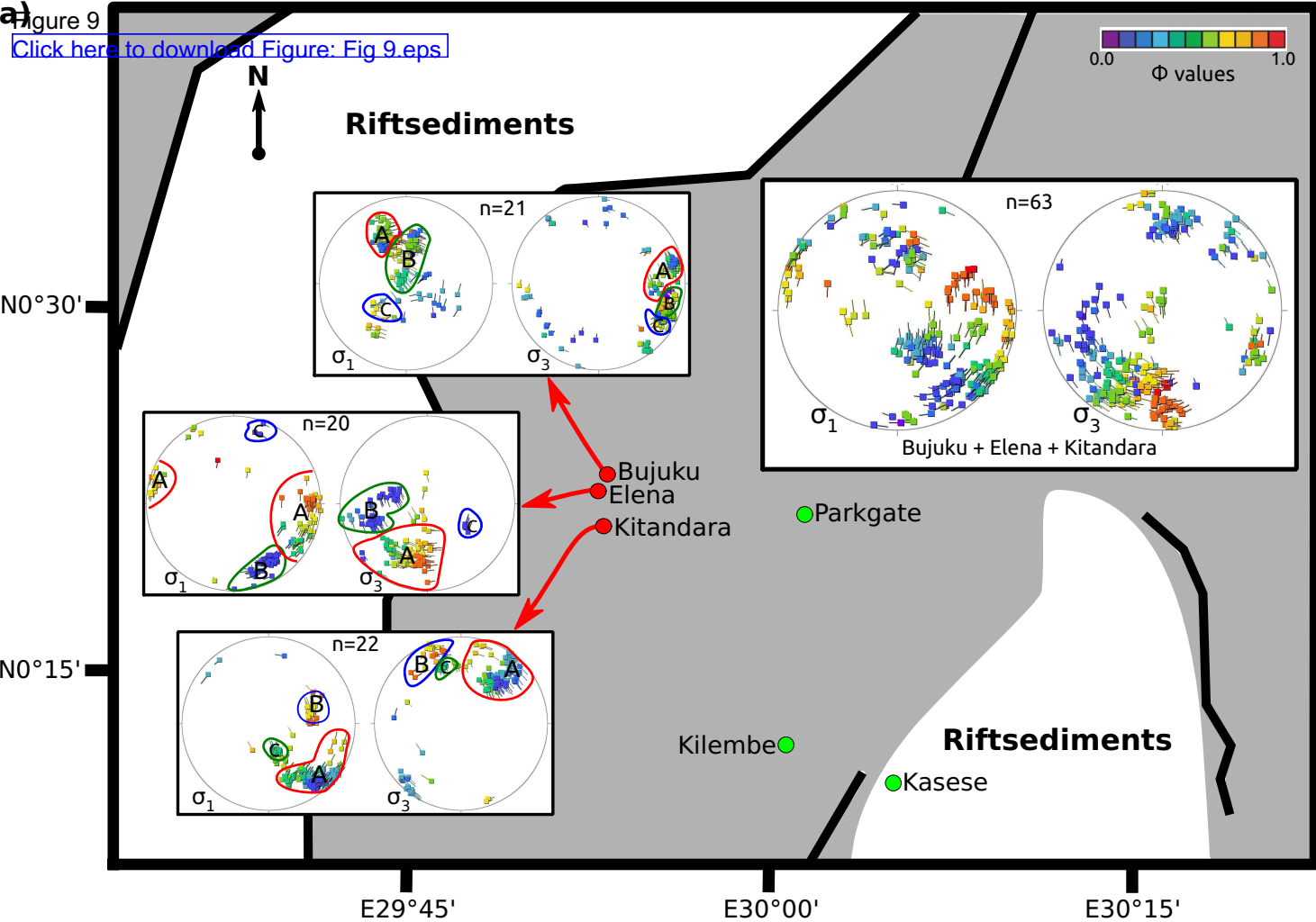


b)



a) Figure 9

[Click here to download Figure: Fig 9.eps](#)



b)

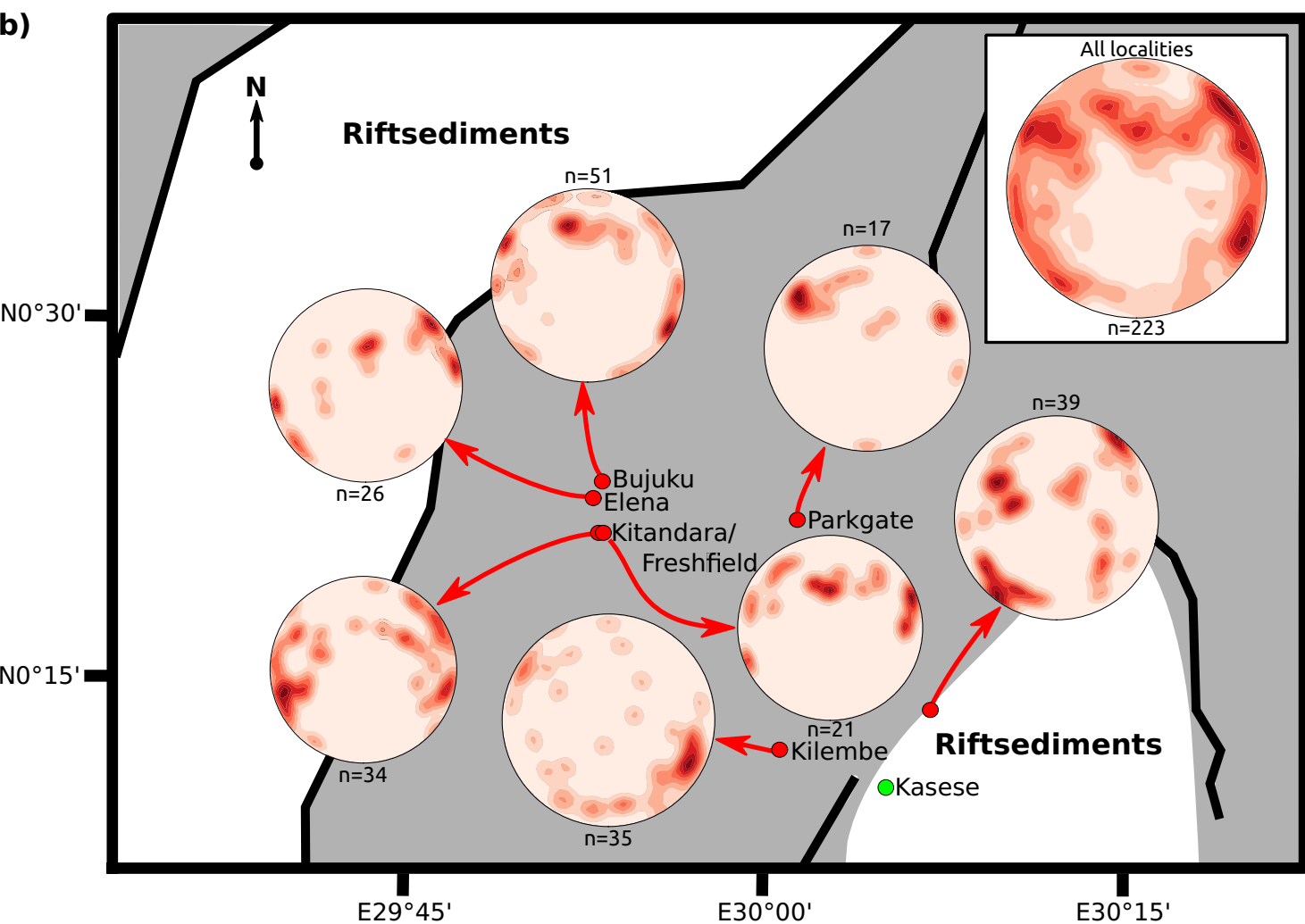


Figure 10

[Click here to download Figure: Fig_10.eps.](#)

